AGU100 ADVANCING EARTH AND SPACE SCIENCE

Geophysical Research Letters

RESEARCH LETTER
10.1029/2018GL078900

Key Points:
- We evaluate the effect of slab deformation on the onset of crack propagation in buried weak snow layers using the finite element method
- The critical crack length for the onset of crack propagation decreases with increasing slope angle
- Slab bending, induced by weak layer collapse, is essential for crack propagation from flat terrain and thus remote avalanche triggering

Correspondence to:
J. Gaume,
johan.gaume@gmail.com

Citation:
Gaume, J., Chambon, G., van Herwijnen, A., & Schweizer, J. (2018). Stress concentrations in weak snowpack layers and conditions for slab avalanche release. *Geophysical Research Letters*, *45*, 8363–8369. https://doi.org/10.1029/2018GL078900

Received 28 MAY 2018
Accepted 16 JUL 2018
Accepted article online 24 JUL 2018
Published online 30 AUG 2018

Stress Concentrations in Weak Snowpack Layers and Conditions for Slab Avalanche Release

J. Gaume[1,2], G. Chambon[3], A. van Herwijnen[2], and J. Schweizer[2]

[1]School of Architecture, Civil and Environmental Engineering, Swiss Federal Institute of Technology EPFL, Lausanne, Switzerland, [2]WSL Institute for Snow and Avalanche Research SLF, Davos, Switzerland, [3]Université Grenoble Alpes, IRSTEA UR ETGR, Grenoble, France

Abstract Dry-snow slab avalanches release due to the formation of a crack in a weak layer buried below cohesive snow slabs, followed by rapid crack propagation. The onset of rapid crack propagation occurs if stresses at the crack tip in the weak layer overcome its strength. In this study, we use the finite element method to evaluate the maximum shear stress τ_{max} induced by a preexisting crack in a weak snow layer allowing for the bending of the overlaying slab. It is shown that τ_{max} increases with increasing crack length, slab thickness, slab density, weak layer elastic modulus, and slope angle. In contrast, τ_{max} decreases with increasing elastic modulus of the slab. Assuming a realistic failure envelope, we computed the critical crack length a_c for the onset of crack propagation. The model allows for remote triggering from flat (or low angle) terrain. Yet it shows that the critical crack length decreases with increasing slope angle.

Plain Language Summary Dry-snow slab avalanches release due to the formation of a crack in a weak layer buried below cohesive snow slabs, followed by rapid crack propagation. Characterizing conditions for the onset of crack propagation in snow is a great challenge and has been the subject of several investigations. Yet there is still no consensus about the nature of the initial failure in the weak layer, whether it occurs in shear only or if the collapse of the weak layer helps to drive crack propagation. Here, to investigate this question, we employed a numerical model to study stress concentrations in the weak layer in the presence of a preexisting crack, allowing the bending of the overlaying slab. We computed the maximum shear stress close to the crack tip for different system configurations and mechanical properties. We showed that steeper slopes promote crack propagation as predicted by classical shear models. However, the collapse of the weak layer is essential for crack propagation from flat terrain and thus remote avalanche triggering.

1. Introduction

A dry-snow slab avalanche originates due to the initiation of a failure in a weak snow layer buried below a cohesive slab, followed by the onset of rapid crack propagation within the weak layer (McClung, 1979; Schweizer et al., 2003; Schweizer, Reuter, van Herwijnen, Richter, & Gaume, 2016). Our understanding of failure initiation has greatly improved over the last decade, in particular, thanks to laboratory and field experiments on snow failure (Chandel et al., 2015; Reiweger & Schweizer, 2010). Recently, Reiweger et al. (2015) characterized the failure envelope of different types of weak layers under mixed-mode loading. Their work confirmed that failure initiation in weak snow layers is more likely under shear than compressive stresses. On the other hand, our knowledge about crack propagation has significantly increased as well due to extensive field work (Bair et al., 2012; Birkeland et al., 2014; Gauthier & Jamieson, 2008; Schweizer, Reuter, van Herwijnen, & Gaume, 2016; van Herwijnen et al., 2016, 2010) and the development of theoretical and numerical models of deformation and fracture in snow (Chiaia et al., 2008; Gaume et al., 2013, 2014, 2017; Gaume, Chambon, et al., 2015; Gaume, van Herwijnen, et al., 2015; Heierli et al., 2008; Monti et al., 2016). However, the two most recent and comprehensive studies that investigated the conditions for the onset of crack propagation led to contrasting results concerning the effect of slope angle. The so-called anticrack model of Heierli et al. (2008) was the first to explain crack propagation on low-angle terrain. They showed that the critical crack length is almost independent of slope angle by assuming a rigid weak layer and a slope independent failure criterion. In contrast, Gaume et al. (2017) developed the shear collapse model (SCM) and showed that the critical crack length a_c decreased with increasing slope angle by accounting for a more realistic behavior of the weak layer. The

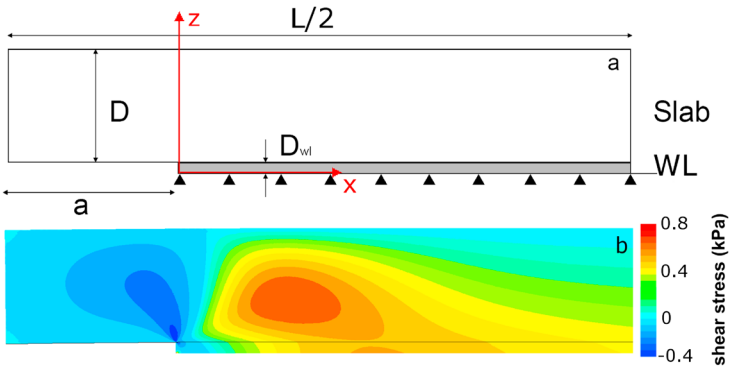

Figure 1. (a) Model geometry. Black triangles represent the fixed boundary condition. (b) Example of shear stress distribution for $a = 0.3$ m, $\rho = 250$ kg/m^3, $\psi = 40°$, $D = 0.2$ m, $E = 10$ MPa, and $E_{wl} = 1$ MPa. The displacement was multiplied by a factor of 10 to discern slab bending. The total length of the system is $L = 2$ m, but only half of it is shown.

maximum shear stress τ_{max}^{SCM} derived by Gaume et al. (2017) based on numerical simulations is as follows:

$$\tau_{max}^{SCM} = \tau\left(1 + \frac{a}{\Lambda}\right) + \frac{1}{2}\sigma\left(\frac{a}{\Lambda}\right)^2, \tag{1}$$

where τ and σ are the shear and normal stresses acting on the weak layer far from the crack, respectively, a is the crack length, and Λ is a characteristic length of the system (see below). SCM is also able to explain fractures on low-angle terrain ($\tau \to 0$) and remote triggering of avalanches and provides similar results as the original shear model (McClung, 1979) for steep terrain (>30°). However, the analytical expression for the maximum shear stress in the weak layer based on critical crack length measurements could not directly be evaluated from the simulations due to the discrete nature of the modeled weak layer. Moreover, van Herwijnen et al. (2016) recently showed using the finite element method (FEM) that in the anticrack model, the mechanical energy of the slab is generally underestimated, except for low slope angles.

To address these controversial findings, we employed a quasi-static finite element model of a slab overlaying a weak layer with a preexisting crack. We computed the shear stress in the weak layer for different snowpack configurations and mechanical properties of the slab and the weak layer, which are treated as linear elastic materials. The comparison to strength measurements of the weak layer allowed to evaluate the critical crack length for the onset of crack propagation.

2. Methods

We used the finite element code Cast3M (Verpeaux et al., 1988). The mass and momentum conservation equations are solved under the hypotheses of small deformations and quasi-static behavior.

The system considered is a two-dimensional (plane stress conditions) propagation saw test (PST) inclined at an angle ψ, of length $L = 2$ m (Figure 1). The choice for the system length was based on the recommendations by Bair et al. (2014) and Gaume, van Herwijnen, et al. (2015) to avoid boundary and finite length effects. The x axis is in the slope-parallel direction, and the z axis is orthogonal to the slope. The system consists of a slab of thickness D overlying a weak layer, in which a preexisting crack of length a is assumed. The mesh size is $r = 5 \times 10^{-4}$ m. We used triangular elements with six Gauss points for the slab and the weak layer (TRI6).

The boundary conditions are as follows: The bottom of the weak layer is fixed and the left and right slope-normal faces of the slab are free, similar to a PST setup (Gauthier & Jamieson, 2008; Sigrist & Schweizer, 2007).

We compute the maximum shear stress τ_{max} found in the weak layer in the vicinity of the crack tip (Figure 1) for given snowpack properties, which were varied independently. Note that we do no consider the shear stress

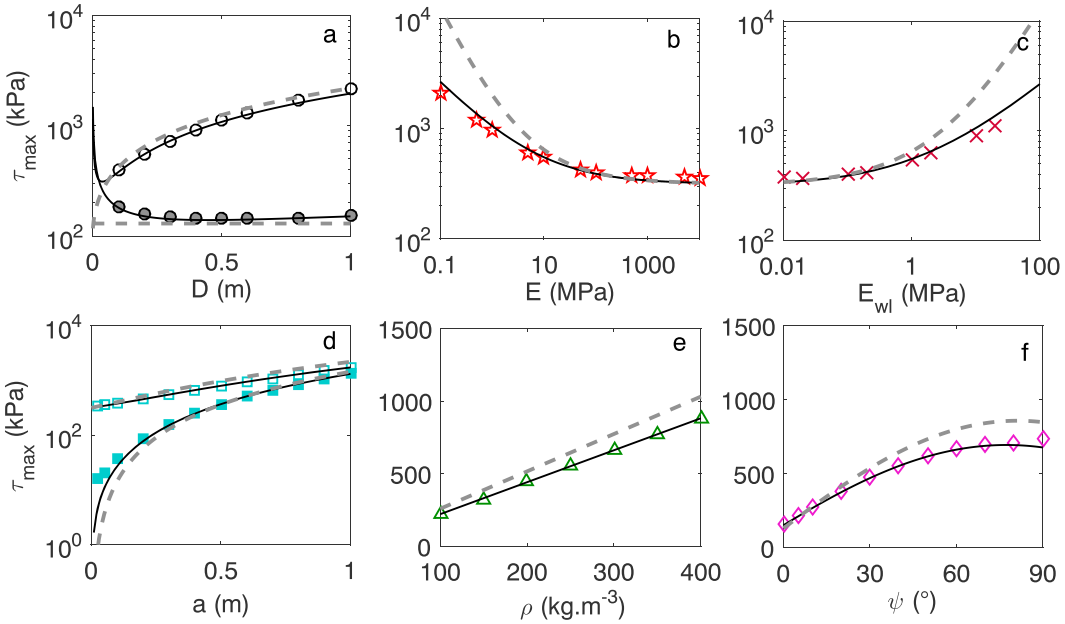

Figure 2. Maximum shear stress τ_{max} as a function of (a) slab thickness D, (b) slab elastic modulus E, (c) weak layer elastic modulus E_{wl}, (d) crack length a, (e) slab density ρ, and (f) slope angle ψ. Symbols: τ_{max}^{FEM}; continuous black line: τ_{max}^{mod} (equation (2); dashed gray line: τ_{max}^{SCM} (equation (1) (Gaume et al., 2017). System properties (if not varied): $a = 0.3$ m, $D = 0.2$ m, $\rho = 250$ kg/m^3, $E = 10$ MPa, $E_{wl} = 1$ MPa for $\psi = 0°$ (full symbols), and $\psi = 40°$ (open symbols).

exactly at the crack tip as its value strongly depends on the mesh resolution. We verified that the value of the maximum shear stress τ_{max} is mesh independent.

3. Results

3.1. Stress Concentration

The maximum shear stress τ_{max} found in the weak layer in the vicinity of the crack tip was evaluated as a function of snowpack properties (Figure 2). The FEM simulations showed that τ_{max} slightly decreases with increasing slab thickness D for $\psi = 0°$. For a steep slope ($\psi = 40°$), τ_{max} increases with increasing slab thickness and is about 1 order of magnitude larger than for $\psi = 0°$. Furthermore, τ_{max} increases with increasing crack length a for any value of slope angle. With increasing elastic modulus of the slab E, the maximum shear stress decreases but increases with increasing weak layer elastic modulus E_{wl}. As expected, τ_{max} increases linearly with increasing slab density ρ. Finally, τ_{max} increases with increasing slope angle.

To explain the observed trends, we derived an analytical expression for the maximum stress based on FEM results. Previous work showed that the maximum stress at the crack tip was primarily a function of the normal stress $\sigma = \rho g D \cos\psi$, the shear stress $\tau = \rho g D \sin\psi$ and the ratios a/Λ and $(a/\Lambda)^2$ (Gaume et al., 2017), where g is the gravitational acceleration. Here $\Lambda = (E' D D_{wl}/G_{wl})^{1/2}$ is a characteristic length of the system associated with the elastic mismatch between the slab and the weak layer, $E' = E/(1-\nu^2)$ and with the shear modulus of the weak layer $G_{wl} = E_{wl}/(2(1+\nu))$; where ν is the Poisson's ratio. Gaume et al. (2017) suggested that additional terms might improve the accuracy of their analytical model; hence, we fitted the following analytical expression to FEM results, including a coupled term $a^2/(\Lambda D)$:

$$\tau_{max}^{mod} = \tau\left[1 + \alpha\frac{a}{\Lambda}\right] + \sigma\left[\beta\frac{a}{\Lambda} + \gamma\frac{a^2}{\Lambda D} + \delta\left(\frac{a}{\Lambda}\right)^2\right]. \quad (2)$$

The best fit was obtained for $\alpha = 0.56$, $\beta = 0.14$, and $\gamma = 0.21$ and $\delta = 0$.

The modeled maximum shear stress τ_{max}^{mod} is also shown in Figure 2 as a function of snowpack properties and in Figure 3 as a function of the FEM maximum shear stress τ_{max}^{FEM}. A good agreement between analytical (equation (2)) and FEM values of τ_{max} is found, except for very low values of the slab elastic modulus and/or very high values of the weak layer elastic modulus where the shear stress is slightly overestimated. In addi-

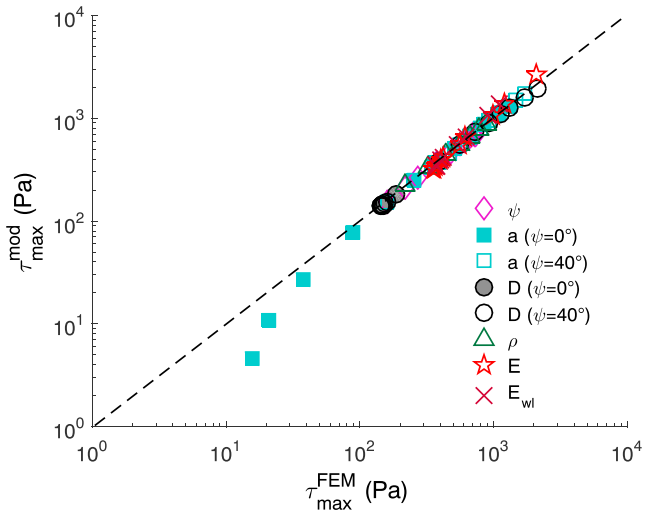

Figure 3. Modeled (equation (2)) τ_{max}^{mod} versus simulated (FEM) τ_{max}^{FEM} maximum shear stress for all the simulated configurations shown in Figure 2. Symbols and colors correspond to those used in Figure 2. The dashed line represents the 1:1 line. FEM = finite element method.

tion, for very short crack lengths ($a \leq 0.1$ m) and $\psi = 0°$, equation (2) slightly underestimates τ_{max} probably due to edge effects as τ_{max} tends to 0.

3.2. Condition for the Onset of Crack Propagation

We assume that the onset of crack propagation occurs when the shear stress at the crack tip in the weak layer reaches the shear strength τ_p, that is, when $\tau_{max} = \tau_p$. When this criterion is met, the crack size corresponds to the so-called critical crack length a_c. The shear strength of persistent weak snow layers (natural and artificially grown faceted crystals, depth hoar, and surface hoar) was measured in laboratory experiments for different loading angles and rates (Reiweger & Schweizer, 2010; Reiweger et al., 2015). It was shown in particular that for realistic values of the normal stress σ, τ_p increased with increasing values of σ (Figure 4, inset). Reiweger et al. (2015) proposed to relate the shear strength to the normal stress according to a Mohr-Coulomb criterion:

$$FC_1: \tau_{p_1} = c_1 + \sigma \tan(\phi) \tag{3}$$

with $c_1 = 170$ Pa and $\phi = 20°$.

This experimentally based relationship for τ_p allows to compute the critical crack length by combining equations (2) and (3). The critical crack length decreases significantly with increasing slope angle ψ (Figure 4), and the snowpack becomes naturally unstable for $\psi > 45°$ ($a_c = 0$, $\tau > \tau_p$).

However, Reiweger et al. (2015) and Chandel et al. (2015) showed that the shear strength of weak snow layers may also decrease for larger values of σ (closed failure envelope). Hence, the dependence with slope angle was also tested for two other simple failure criteria represented in Figure 4 (inset), one in which the shear strength τ_p is independent of the normal stress σ and one for which τ_p decreases with increasing σ:

$$FC_2: \tau_{p_2} = c_2, \tag{4}$$

$$FC_3: \tau_{p_3} = c_3 - \sigma \tan(\phi), \tag{5}$$

with $c_2 = 600$ Pa and $c_3 = 1{,}050$ Pa.

For all failure criteria, the simulated critical crack length a_c decreases with increasing slope angle, although the decrease is less pronounced for the criterion FC_3 for which a_c levels off for a slope angle around 40°. Criterion FC_1 yields a lower critical crack length than FC_2, which is itself lower than FC_3 since $\tau_{p_1} < \tau_{p_2} < \tau_{p_3}$ in the range of normal stress values used ($\sigma < 1$ kPa).

4. Discussion

The findings of Heierli et al. (2008; anticrack model) and Gaume et al. (2017; SCM) showed contradictory results on the effect of slope angle on the onset of crack propagation in weak snow layers. Hence, in a typical

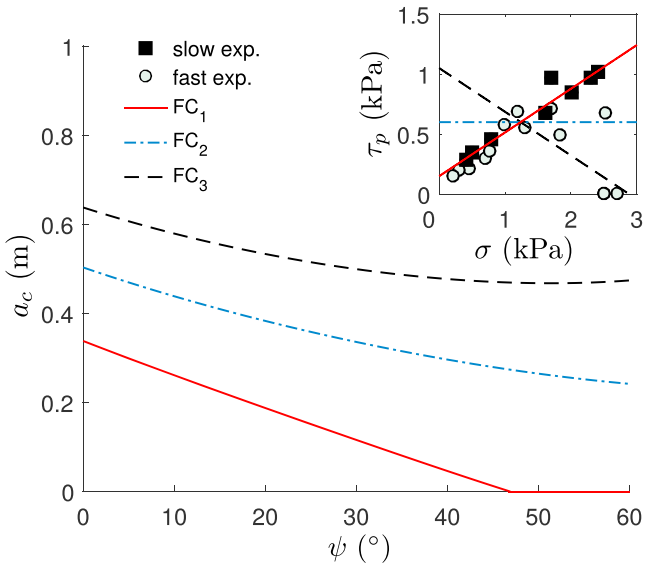

Figure 4. Critical crack length a_c as a function of slope angle. Inset: Shear strength of weak snow layers obtained with laboratory experiments (Reiweger et al., 2015) for fast (circles) and slow (squares) experiments. The solid line (FC_1) represents a linear fit (Mohr-Coulomb) to the experimental data used to compute a_c. FC_2 and FC_3 are two other hypothetical failure criteria (see text). System properties: $\rho = 180$ kg/m^3, $E = 2$ MPa, $D = 0.2$ m, $D_{wl} = 0.02$ m, and $G_{wl} = 0.4$ MPa.

slab-weak layer configuration, we computed the maximum shear stress at the crack tip using a finite element model, which was not directly possible in Gaume et al. (2017) because of the discrete nature of the weak layer. Our new model based on FEM confirms the recent results of Gaume et al. (2017) predicting that the critical crack length decreases with increasing slope angle, in contrast to the anticrack model of Heierli et al. (2008) who obtained a critical crack length independent of slope angle. We also show that the assumption for the failure criterion of the weak layer does not strongly affect the general decreasing trend of the critical crack length with increasing slope angle. Hence, we suggest two main reasons for the discrepancy with the anticrack model:

1. The anticrack model assumes a rigid weak layer to evaluate the mechanical energy of the slab. Hence, the elastic mismatch between the slab and the weak layer is not accounted for.
2. The mechanical energy derived in the anticrack model does not correctly reproduce the interplay between slab bending and tension under mixed-mode loading. Indeed, van Herwijnen et al. (2016) recently showed using FEM that the mechanical energy of the slab was generally underestimated, except for low slope angles.

Our analytical model (equation (2)) also slightly differs from SCM (Gaume et al., 2017). In particular, in the SCM, the maximum shear stress at the crack tip was related to a/Λ and $(a/\Lambda)^2$ only. However, here, the maximum shear stress also depends on an additional coupled term $a^2/(\Lambda D)$. This probably explains the difference observed for the influence of slab and weak layer elastic moduli (Figures 2b and 2c). Nevertheless, for realistic elastic moduli of the slab and the weak layer ($E \in [1-20]$ MPa and $E_{wl} \in [0.05-2]$ MPa), both models yield very similar results in terms of maximum shear stress τ_{max} and thus of absolute value of the critical crack length a_c (Figures 2b and 2c). Concerning the other mechanical properties of the system, our new model and the SCM (Gaume et al., 2017) yield very similar results with consistent trends (Figure 2), although some slight quantitative discrepancies are observed (Figures 2e and 2f).

The maximum shear stress at the crack tip of the weak layer was evaluated assuming a purely linear elastic and isotropic behavior of both the slab and the weak layer before failure. We made this choice as we wanted to focus on the onset of crack propagation in the weak layer only. Nevertheless, the same model could be used to check whether tensile stresses in the slab exceeded the tensile strength to evaluate if the slab would fracture before the onset of crack propagation (Reuter & Schweizer, 2018). As shown by Gaume, van Herwijnen, et al. (2015), slab fractures rarely occur before the onset of crack propagation, except for very soft slabs ($\rho < 150$ kg/m^3). For the weak layer, the isotropic elastic character is probably not very realistic since these layers are probably stiffer in compression than in shear. Although failure anisotropy was accounted for through the fail-

ure envelope, an orthotropic elastic behavior with different elastic moduli in the different loading directions (Srivastava et al., 2016; Walters & Adams, 2014) might be more appropriate.

Reiweger et al. (2015) evaluated the failure envelope of weak snowpack layers, that is, the strength under different loading conditions. They showed that weak layer strength can be described by a Mohr-Coulomb criterion for typical values of normal stress encountered in the field. Hence, the shear strength increases with increasing normal stress σ. However, for large values of σ, snow can exhibit compressive failures leading to a decrease of the shear strength with increasing σ. Furthermore, Chandel et al. (2015) described weak layers for which the shear strength always decreases with increasing σ. These discrepancies reveal the strong variability of weak snow layers, such that there is probably no unique failure criterion describing all types of weak layers. Nevertheless, although the absolute strength value has a strong influence on the critical crack length, our model suggests that the trend of weak layer strength with slope angle ψ does not significantly affect the trend of the critical crack length with ψ (Figure 4). However, a decreasing trend of weak layer strength with σ leads to a gentler decrease of a_c with slope angle.

Concerning size effects, we checked that our results obtained for realistic snowpack properties are uninfluenced by the system length L. Typically, to prevent size effects, the condition $(a + \Lambda)/L \ll 1$ must be fulfilled. In our simulations, this ratio is generally lower than 0.3 except for combinations of large crack lengths ($a > 0.5$ m) and very large slab elastic moduli ($E > 50$ MPa). In that case $(a + \Lambda)/L$ can reach ~0.5 for which size effects occur. Nevertheless, these values of crack length and slab elastic modulus are larger than the ones typically encountered in the field.

Finally, we consider here a PST configuration with a preexisting crack, which is different from a real slab avalanche scenario. In a PST, the crack in the weak layer is artificially made using a saw. However, in the case of a skier-triggered slab avalanche, the skier directly induces a failure in the weak layer below his skis (Schweizer & Jamieson, 2001). Recently, Gaume and Reuter (2017) developed a new model for skier-triggered avalanches that compares the critical crack length obtained in a PST to the so-called skier crack length, that is, the size of the area where the skier-induced stress exceeds the shear strength of the weak layer. As previously suggested by Schweizer and Jamieson (2001), Gaume and Reuter (2017) confirmed that a skier does not need to hit a (hypothetical) preexisting crack in the weak layer to trigger a slab avalanche.

5. Conclusion

We conducted finite element simulations of a snow slab overlaying a weak snow layer in which a preexisting crack was assumed allowing for slab tension and bending. We computed the maximum shear stress τ_{max} as a function of snowpack properties. A parametric analysis evidenced that τ_{max} increases with increasing crack length, slab thickness, slab density, weak layer elastic modulus, and slope angle. On the other hand, τ_{max} decreases with increasing elastic modulus of the slab. The critical crack length for the onset of crack propagation was evaluated by comparing the maximum shear stress to strength values obtained with snow failure experiments. The process of initiating and propagating cracks on flat terrain and thus remote triggering of avalanches can be explained by our model in line with the anticrack model. However, our model confirms the recent findings of Gaume et al. (2017) showing that the critical crack length decreases with increasing slope angle. Although the model of Gaume et al. (2017) was in fair agreement with field data, future experimental work is required to confirm our numerical results on the effect of slope angle on crack propagation.

Acknowledgments
Johan Gaume has been supported by the Ambizione grant of the Swiss National Science Foundation (PZ00P2_161329). The Finite Element code Cast3m can be downloaded at http://www-cast3m.cea.fr/. Data and model results can be found on the Zenodo repository (https://doi.org/10.5281/zenodo.1309255).

References

Bair, E. H., Simenhois, R., Birkeland, K., & Dozier, J. (2012). A field study on failure of storm snow slab avalanches. *Cold Regions Science and Technology*, *79*, 20–28.

Bair, E., Simenhois, R., van Herwijnen, A., & Birkeland, K. (2014). The influence of edge effects on crack propagation in snow stability tests. *The Cryosphere*, *8*, 1407–1418.

Birkeland, K., van Herwijnen, A., Knoff, E., Staples, M., Bair, E., & Simenhois, R. (2014). The role of slab and weak layers in fracture arrest. In P. Haegeli (Ed.), *2014 International Snow Science Workshop* (pp. 156–163). Banff, Alberta.

Chandel, C., Srivastava, P. K., & Mahajan, P. (2015). Determination of failure envelope for faceted snow through numerical simulations. *Cold Regions Science and Technology*, *116*, 56–64.

Chiaia, B., Cornetti, P., & Frigo, B. (2008). Triggering of dry snow slab avalanches: Stress versus fracture mechanical approach. *Cold Regions Science and Technology*, *53*, 170–178.

Gaume, J., Chambon, G., Eckert, N., & Naaim, M. (2013). Influence of weak-layer heterogeneity on snow slab avalanche release: Application to the evaluation of avalanche release depths. *Journal of Glaciology*, *59*(215), 423–437.

Gaume, J., Chambon, G., Eckert, N., Naaim, M., & Schweizer, J. (2015). Influence of weak layer heterogeneity and slab properties on slab tensile failure propensity and avalanche release area. *The Cryosphere*, *9*(2), 795–804. https://doi.org/10.5194/tc-9-795-2015

Gaume, J., & Reuter, B. (2017). Assessing snow instability in skier-triggered snow slab avalanches by combining failure initiation and crack propagation. *Cold Regions Science and Technology*, *114*, 6–15.
Gaume, J., Schweizer, J., van Herwijnen, A., Chambon, G., Reuter, B., Eckert, N., & Naaim, M. (2014). Evaluation of slope stability with respect to snowpack spatial variability. *Journal of Geophysical Research: Earth Surface*, *119*, 1783–1789. https://doi.org/10.1002/2014JF003193,
Gaume, J., van Herwijnen, A., Chambon, G., Birkeland, K., & Schweizer, J. (2015). Modeling of crack propagation in weak snowpack layers using the discrete element method. *The Cryosphere*, *9*, 1915–1932.
Gaume, J., van Herwijnen, A., Chambon, G., Wever, N., & Schweizer, J. (2017). Snow fracture in relation to slab avalanche release: Critical state for the onset of crack propagation. *The Cryosphere*, *11*, 217–228. https://doi.org/10.5194/tc-2016-64
Gauthier, D., & Jamieson, B. (2008). Evaluation of a prototype field test for fracture and failure propagation propensity in weak snowpack layers. *Cold Regions Science and Technology*, *51*(2), 87–97.
Heierli, J., Gumbsch, P., & Zaiser, M. (2008). Anticrack nucleation as triggering mechanism for snow slab avalanches. *Science*, *321*, 240–243.
McClung, D. (1979). Shear fracture precipitated by strain softening as a mechanism of dry slab avalanche release. *Journal of Geophysical Research*, *84*(B7), 3519–3526.
Monti, F., Gaume, J., Van Herwijnen, A., & Schweizer, J. (2016). A simplified approach to assess the skier-induced stress within a multi-layered snowpack. *Natural Hazards and Earth System Sciences*, *16*, 775–788.
Reiweger, I., Gaume, J., & Schweizer, J. (2015). A new mixed-mode failure criterion for weak snowpack layers. *Geophysical Research Letters*, *42*, 1427–1432. https://doi.org/10.1002/2014GL062780
Reiweger, I., & Schweizer, J. (2010). Failure of a layer of buried surface hoar. *Geophysical Research Letters*, *37*, L24501.
Reuter, B., & Schweizer, J. (2018). Describing snow instability by failure initiation, crack propagation and slab tensile support. *Geophysical Research Letters*, *45*. https://doi.org/10.1029/2018GL078069
Schweizer, J., & Jamieson, J. (2001). Snow cover properties for skier triggering of avalanches. *Cold Regions Science and Technology*, *33*(2), 207–221.
Schweizer, J., Jamieson, B., & Schneebeli, M. (2003). Snow avalanche formation. *Reviews of Geophysics*, *41*(4), 1016. https://doi.org/10.1029/2002RG000123
Schweizer, J., Reuter, B., van Herwijnen, A., & Gaume, J. (2016). Avalanche release 101. In E. Greene (Ed.), *Proceedings ISSW 2016. International Snow Science Workshop* (pp. 1–11). Breckenridge, CO. 04-08 October 2016.
Schweizer, J., Reuter, B., van Herwijnen, A., Richter, B., & Gaume, J. (2016). Temporal evolution of crack propagation propensity in snow in relation to slab and weak layer properties. *The Cryosphere*, *10*(6), 2637–2653. https://doi.org/10.5194/tc-10-2637-2016,
Sigrist, C., & Schweizer, J. (2007). Critical energy release rates of weak snowpack layers determined in field experiments. *Geophysical Research Letters*, *34*, L03502. https://doi.org/10.1029/2006GL028576
Srivastava, P. K., Chandel, C., Mahajan, P., & Pankaj, P. (2016). Prediction of anisotropic elastic properties of snow from its microstructure. *Cold Regions Science and Technology*, *125*, 85–100. https://doi.org/10.1016/j.coldregions.2016.02.002
van Herwijnen, A., Gaume, J., Bair, E. H., Reuter, B., Birkeland, K. W., & Schweizer, J. (2016). Estimating the effective elastic modulus and specific fracture energy of snowpack layers from field experiments. *Journal of Glaciology*, *62*(236), 997–1007.
van Herwijnen, A., Schweizer, J., & Heierli, J. (2010). Measurement of the deformation field associated with fracture propagation in weak snowpack layers. *Journal of Geophysical Research*, *115*, F03042. https://doi.org/10.1029/2009JF001515
Verpeaux, P., Charras, T., & Millard, A. (1988). Castem2000: une approche moderne du calcul des structures, Calcul des structures et intelligence artificielle (Ed. Pluralis).
Walters, D. J., & Adams, E. E. (2014). Quantifying anisotropy from experimental testing of radiation recrystallized snow layers. *Cold Regions Science and Technology*, *97*, 72–80.